Radiology: Imaging Cancer

ORIGINAL RESEARCH

Tumor Biomechanics Quantified Using MR Elastography to Predict Response to Neoadjuvant Chemotherapy in Individuals with Breast Cancer

Aaditya P. Sinha, MD(Res)[*1,2] • *Patriek Jurrius, PhD*[*1,2] • *Anne-Sophie van Schelt, PhD*[3] • *Omar Darwish, PhD*[3] • *Belul Shifa, MSc*[2] • *Giacomo Annio, PhD*[4] • *Zhane Peterson, BSc*[2] • *Hannah Jeffery, MRCS*[1,2] • *Karen Welsh, BSc*[3,5] • *Anna Metafa, FRCR*[6] • *John Spence, BSc*[5] • *Ashutosh Kothari, FEBS*[2] • *Hisham Hamed, PhD*[2] • *Georgina Bitsakou, PhD*[2] • *Vasileios Karydakis, PhD*[2] • *Mangesh Thorat, PhD*[2] • *Elina Shaari, MRCS*[2] • *Ali Sever, PhD*[2] • *Anne Rigg, PhD*[2] • *Tony Ng, PhD*[1] • *Sarah Pinder, PhD*[1,2] • *Ralph Sinkus, PhD*[**3,4] • *Arnie Purushotham, MD*[**1,2]

* A.P.S. and P.J. contributed equally to this work.

** R.S. and A.P. are co–senior authors.

Author affiliations, funding, and conflicts of interest are listed at the end of this article.

Radiology: Imaging Cancer 2025; 7(2):e240138 • https://doi.org/10.1148/rycan.240138 • Content codes: BR MR OI

Purpose: To evaluate the ability of MR elastography (MRE) to noninvasively quantify tissue biomechanics and determine the added diagnostic value of biomechanics for predicting response throughout neoadjuvant chemotherapy (NAC).

Materials and Methods: In this prospective study (between September 2020 and August 2023; registration no. NCT03238144), participants with breast cancer scheduled to undergo NAC underwent five MRE scans at different time points alongside clinical dynamic contrast-enhanced MRI (DCE MRI). Regions of interest were drawn over the tumor region for the first two scans, while for the post-NAC scan, the initial pre-NAC tumor footprint was used. Biomechanics, specifically tumor stiffness and phase angle within these regions of interest, were quantified as well as the corresponding ratios relative to before NAC (tumor-stiffness ratio and phase-angle ratio, respectively). Postsurgical pathologic analysis was used to determine complete and partial responders. Furthermore, a repeatability analysis was performed for 18 participants.

Results: Datasets of 41 female participants (mean age, 47 years ± 12.5 [SD]) were included in this analysis. The tumor-stiffness ratio following NAC decreased significantly for complete responders and increased for partial responders (0.76 ± 0.16 and 1.14 ± 0.24, respectively; $P < .001$). The phase-angle ratio after the first cycle of the first NAC regimen compared with before NAC predicted pathologic response (1.23 ± 0.31 vs 0.91 ± 0.34; $P < .001$). Combining the tumor stiffness ratio with DCE MRI improved specificity compared with DCE MRI alone (96% vs 44%) while maintaining the high sensitivity of DCE MRI (94%). Repeatability analysis showed excellent agreement for elasticity (repeatability coefficient, 8.3%) and phase angle (repeatability coefficient, 5%).

Conclusion: MRE–derived phase-angle ratio and tumor stiffness ratio were associated with pathologic complete response in participants with breast cancer undergoing NAC, and a combined DCE MRI plus MRE approach significantly enhanced specificity for identification of complete responders after NAC, while maintaining high sensitivity.

Supplemental material is available for this article.

Clinical trials registration no. NCT03238144

Breast cancer is a common disease globally, with 2.3 million diagnoses annually and a lifetime risk of one in seven women in the United Kingdom (1,2). The high prevalence rate makes it the most common cancer in women and the second most common cause of cancer death for women globally (3). Neoadjuvant chemotherapy (NAC) is the primary systemic therapy to downsize solid tumors, after which most patients undergo (breast-conserving) surgery. Currently, the residual cancer burden (RCB) scoring system at final histopathologic analysis is used to predict disease recurrence and survival rates. However, this is not applicable during ongoing treatment with NAC (4). Throughout therapy, breast MRI with dynamic contrast enhancement (DCE) is used as the current reference standard in assessing response clinically, with a sensitivity of typically 80% and a specificity ranging from 37% to 97% (5–8). Additionally, radiologic vacuum-assisted biopsies have been used to assess pathologic complete response (pCR). However, using a 14-gauge needle may not be a reliable predictor of pCR (9–11), with different studies reporting false-negative rates as high as 42% due to sampling errors (9). Current research has focused on de-escalation in breast cancer treatment to potentially avoid surgery and change therapy early for nonresponders (12). Thus, a method for accurate monitoring of response is of critical importance.

One promising avenue for assessing response is to investigate tumor biomechanics (13,14). It is known that tissue angiogenesis, lymphangiogenesis, hypoxia, and inflammation all promote tumor aggression, which exerts mechanical forces on the tumor and its microenvironment (15–17). Furthermore, tissue mechanics are modulated by a solid tumors' high interstitial pressure, which impacts hypoxia, metastatic propensity, mortality, and treatment outcome (18). It has been shown that invasive regions exhibit an elevated mean stiffness primarily due to an increase in collagen deposition (19). Consistently,

Abbreviations

DCE = dynamic contrast enhanced, MRE = MR elastography, NAC = neoadjuvant chemotherapy, PAR = phase angle ratio, pCR = pathologic complete response, RCB = residual cancer burden, ROI = region of interest, TSR = tumor stiffness ratio

Summary

Assessment of tumor biomechanics through MR elastography improved the identification of complete responders among individuals with breast cancer undergoing neoadjuvant chemotherapy.

Key Points

- In individuals who underwent MR elastography in addition to dynamic contrast-enhanced (DCE) MRI throughout neoadjuvant chemotherapy (NAC) for breast cancer, a drop in the tumor-stiffness ratio from prior to NAC to after NAC was indicative of pathologic complete response (complete responders, 0.76 ± 0.16 [SD]; partial responders, 1.14 ± 0.24; $P < .001$).
- A combined DCE MRI and MR elastography biomarker approach improved specificity for the identification of complete responders following NAC from 44% (DCE MRI alone) to 96%.
- A rise in biomechanical tumor phase angle ratio from before NAC to the first cycle of NAC was associated with pathologic complete response (complete responders, 1.23 ± 0.31; partial responders, 0.91 ± 0.34; $P < .001$).

Keywords

Breast Cancer, MR Elastography, Neoadjuvant Chemotherapy, Dynamic Contrast-enhanced MRI

unconfined compression analysis shows that tumor stiffness is associated with aggressive cancers (20,21). Therefore, gauging tumor biomechanics noninvasively could be useful for assessment of therapy efficacy.

MR elastography (MRE) is an imaging modality that uses propagating mechanical shear waves to enable noninvasive quantification of tissue biomechanics (22) and has already demonstrated promise in the characterization of breast lesions (23–25). Hence, this study aims to demonstrate *(a)* the feasibility of using MRE as part of clinical breast cancer NAC and *(b)* to investigate the added diagnostic value of biomechanics for predicting response throughout NAC.

Material and Methods

Study Design and Participants

This single-arm phase II prospective study (conducted between September 2020 and August 2023) was approved by an independent review board (reference nos. 16/LO/1303, NCT03238144), and all participants provided written informed consent. Inclusion criteria were female participants aged 18 years or older with invasive breast cancer who were scheduled to undergo NAC and able to provide written informed consent. Exclusion criteria were prior ipsilateral breast cancer, inability to provide written informed consent, and contraindications for MRI. Participant demographics, tumor characteristics, treatment regimens, and radiologic and pathologic responses were recorded. A flowchart of patient inclusion is shown in Figure 1A. All participants underwent surgery after NAC. The breast specimens were assessed for response to NAC using the MD Anderson RCB score (4). The RCB score was categorized as RCB-0 (pCR, RCB = 0), RCB-I (0.5 < RCB ≤ 1.36), RCB-II (1.36 < RCB ≤ 3.28), and RCB-III (RCB > 3.28). This classification allowed for categorizing patients into those who achieved a pCR or partial response (RCB-I, -II, or -III).

MRI plus MRE scans were performed before treatment (pre-NAC), halfway through treatment (mid-NAC), and at the end of treatment (post-NAC) (Fig 1B). Two additional MRE-only scans were performed after the first cycle of the first NAC regimen (postcycle 1.1) and after the second NAC regimen (postcycle 2.1). With the current study aims (ie, gauging pathologic response and identifying potentially early resistance or response), this article focuses on the following three time points: pre-NAC, postcycle 1.1, and post-NAC. In all, 41 participants underwent all five scans, including three clinical DCE MRI acquisitions.

MRE Hardware and Sequencing

Scans were performed using a MAGNETOM Aera 1.5-T MRI system (Siemens Healthineers). Standard MRI protocols were acquired using T1-weighted, T2-weighted, diffusion-weighted, and DCE sequences. To enable MRE, the gravitational transducer (26) was integrated into the Siemens four-channel breast biopsy radiofrequency coil (Fig 2). Participants were positioned prone and head first with the breasts placed in the designated openings of the radiofrequency coil. The gravitational transducer had two rotating eccentric masses generating longitudinal vibrations in feet-head direction (Fig 2A). Mechanical vibrations were transmitted in the breasts through active paddles. Passive paddles, adjustable in the feet-head direction, were used to ensure good mechanical contact between the breasts and active paddles (Fig 2B). The gravitational transducer was connected to the driving motor unit via a 9m flexible rotating axis (Fig 2C). MRE data were acquired using a gradient-echo sequence (eXpresso) (27) at 36 Hz with fractional motion-encoding gradients at 20 mT/m. Imaging parameters were as follows: 16 sections; 3-mm isotropic voxel size; 128 × 128 acquisition matrix; and an in-plane generalized autocalibrating partial parallel acquisition acceleration factor of 2, resulting in a field of view of 384 × 384 × 48 mm^3; echo time of 9.2 msec; repetition time of 222 msec (16 × 13.9 msec); and a flip angle of 25°. The field of view was centered on the tumor core, which was identified using anatomic scans. MRE acquisitions took approximately 7 minutes, with total acquisition times of 25 minutes for clinical scans and 16 minutes for research scans only.

MRE Postprocessing

MRE data were processed according to Sinkus et al (28). In short, applying the curl operator removes contributions from compressional waves from the total wave field. Spatial derivatives necessary to solve the wave equation were calculated in Fourier space to improve quality and robustness. An 11th-order Blackman-Harris filter was applied to suppress noise. Before Fourier transformation, the wave field was smoothed with a Gaussian filter (3 × 3 × 3 pixels stealth, 0.75 pixels sigma). The final three complex-valued equations (Helmholtz-type) are

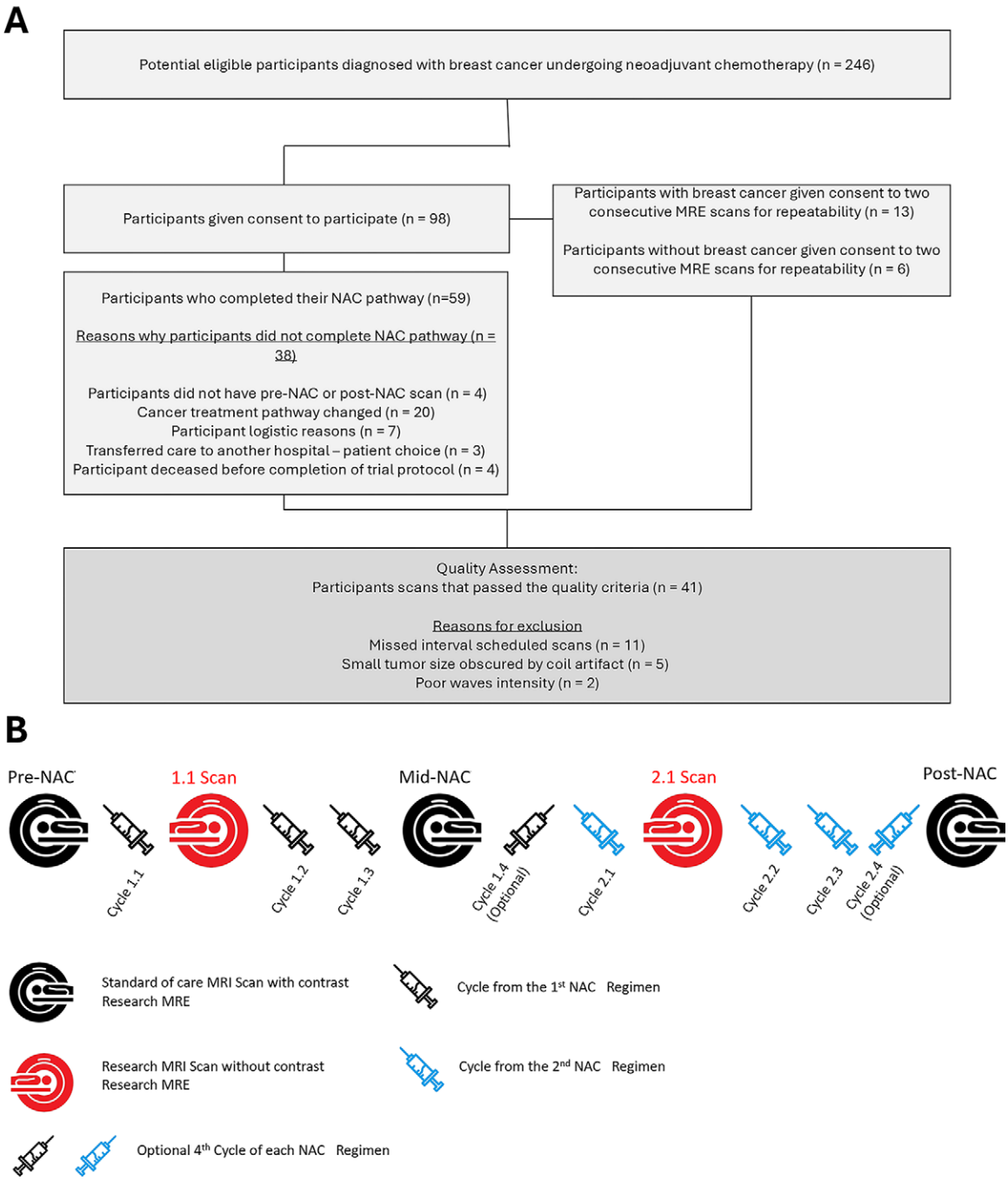

Figure 1: Flowchart and study pathway. **(A)** Flowchart of participant inclusion. Ultimately, datasets from 41 participants who fulfilled all necessary criteria (ie, all scans performed throughout neoadjuvant chemotherapy [NAC], all scans with sufficient quality, and post-NAC histopathologic analyses available) were included in this analysis. **(B)** Participants received three or four cycles of the first regimen and three or four cycles of the second regimen prior to post-NAC surgical intervention. In total, five MRI and MR elastography (MRE) sessions were interlaced with the NAC regimen.

solved for the wave vector $\vec{k}^2 = \frac{\rho\omega^2}{G^*}$ through a χ^2 minimization approach, with ρ the density, ω the circular frequency, and $G^* = G' + iG''$ the complex-valued shear modulus with G' elasticity and G'' viscosity (in kilopascals). From G^* the phase angle $Y = \frac{2}{\pi} atan\left(\frac{G''}{G'}\right) \in [0,1]$ is derived.

MRE Biologic Markers and Statistical Analysis

Regions of interest (ROIs) were drawn by a consultant radiologist (A.M.) with more than 15 years of experience with breast MRI. Guided by standard diagnostic scans, ROIs were placed accordingly on the MRE magnitude images without knowledge of the underlying maps depicting biomechanics. ROIs were drawn over the tumor area for the pre-NAC and postcycle 1.1 MRE, excluding the region of the localization marker clip (see

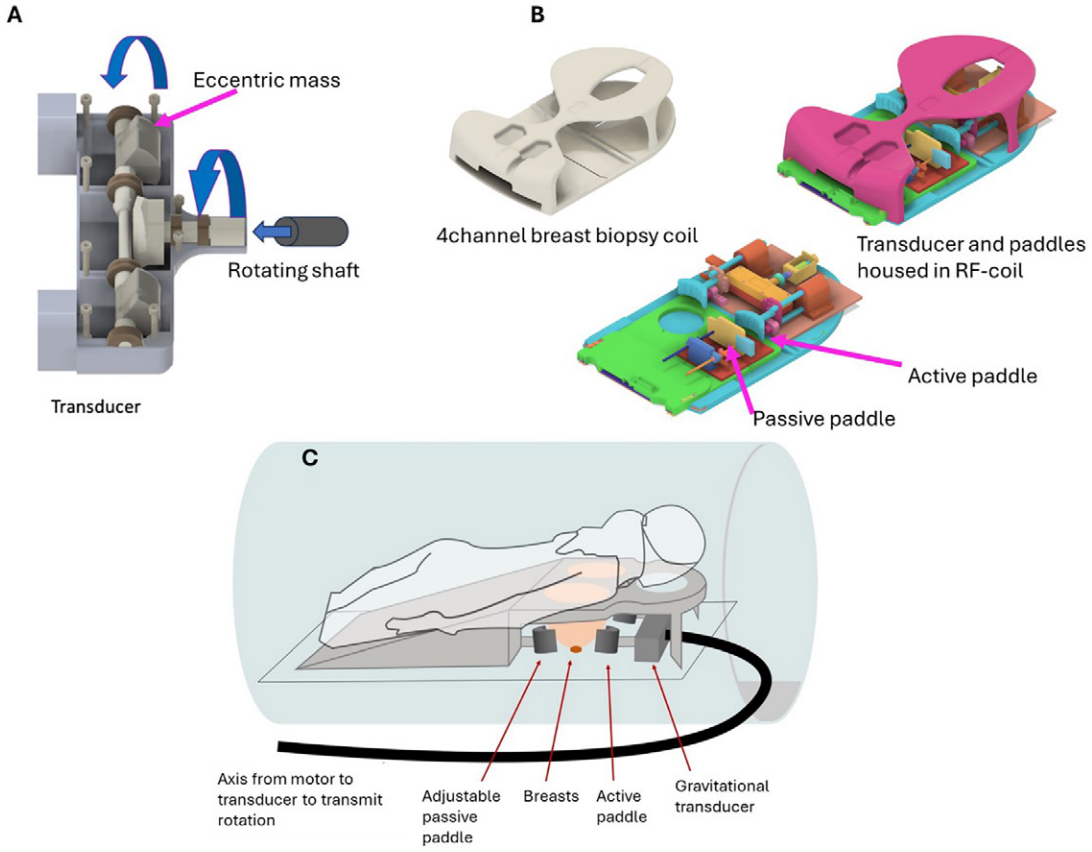

Figure 2: Gravitational transducer (GT) setup for the breast MRI coil. **(A)** The GT-based MR elastography breast setup consists of two eccentric masses that rotate around an axis that is oriented right-left. The flexible shaft that transmits the rotations from the motor to the transducer arrives from the head direction and connects to the transducer via a bayonet connection. **(B)** The entire GT setup is incorporated into the four-channel biopsy coil from Siemens. It hosts the transducer as well as active and passive paddles. The passive paddles are movable in the feet-head direction to ensure that the breasts have proper mechanical contact with the active paddles, which are fixed to the GT and only vibrate and cannot be moved. **(C)** Sketch of the entire setup showing the patient, the paddles, the GT, and the rotating flexible shaft entering from the head side. RF = radiofrequency.

Fig S1). Because after NAC there is frequently no discernible tumor visible anymore (only two participants had discernible tumors), the initial tumor footprint ROI from before NAC was used as a landmark for ROI placement. A more detailed description is provided in Appendix S1.

Biologic markers were quantified within the corresponding ROIs via either the mean value of the distribution in case of tumor elasticity or the mean peak value of a Gaussian or Landau fit for the phase angle (depending on the lowest χ^2 of the fit, correspondingly). In addition to absolute values, ratios of biologic markers were investigated to more easily identify trends among participants and study their temporal evolution throughout therapy. Specifically, we investigated the tumor stiffness ratio (TSR) $\left(TSR = \frac{G'_{1.1\ or\ post-NACT}}{G'_{pre-NACT}}\right)$ and phase angle ratio (PAR) $\left(PAR = \frac{Y_{1.1\ or\ post-NACT}}{Y_{pre-NACT}}\right)$ with their corresponding normalization relative to before NAC.

The TSR is defined as the ratio of elasticity measured after NAC (post-NAC) to the elasticity measured before the treatment (pre-NAC). A TSR greater than 1 indicates a decrease in elasticity over time and that the tissue is less elastic at post-NAC compared with at pre-NAC. Conversely, a TSR less than 1 suggests an increase in elasticity before NAC compared with after NAC. If the elasticity remains unchanged, the TSR will equal 1. The expected range is between 0.1 and 2, where in the most extreme cases the elasticity has a significant drop or a doubling of the initial elasticity observed prior to NAC.

The PAR is defined as the ratio of the phase angle at postcycle 1.1 to the phase angle measured at pre-NAC. A PAR greater than 1 indicates a decrease in phase angle at 1.1 compared with before NAC. A PAR smaller than 1 shows a phase angle increase at 1.1 compared with before NAC. For a PAR of 1, the phase angle remains unchanged. Similarly to the TSR, the more extreme cases could decrease or elevate the ratio to 0.1 or 2, respectively.

Data quality criteria were local shear wave amplitude (Atot ≥ 95 μm), nonlinearity (<35%, which indicates how much the phase signal intensity deviates from a perfect sinusoidal), and the wave signal-to-noise ratio (>3) expressed by the ratio of the magnitude of the wave's rotation over its divergence. Additionally, scans were rejected if the number of exploitable voxels within an ROI dropped below 120 pixels whereby rendering the corresponding biologic markers not statistically reliable (Fig S2). Any tumor region that did not meet these criteria on average was excluded from the analysis.

Independent samples *t* tests or Wilcoxon signed rank tests were used to compare complete and partial responders, depending on normality (Shapiro-Wilk test). Repeatability was assessed using Bland-Altman analysis, intraclass correlation coefficients, and the repeatability coefficient (the full protocol is in Appendix S1). The predictive ability of MRE-derived parameters were assessed using

Table 1: Characteristics of Study Participants

Baseline Characteristic	Value
No. of participants	41
Age (y)	
Mean (SD)	47 (12.5)
Median (Q1, Q3)	48 (35, 55)
Min, max	21, 63
Tumor size at baseline MRI (mm)	
Mean (SD)	43.1 (22.6)
Median (Q1, Q3)	37 (29, 51)
Min, max	8, 110
Histologic tumor grade	
Grade 1	0 (0)
Grade 2	11 (27)
Grade 3	30 (73)
Invasive tumor type	
NST	39 (95)
Mucinous	1 (2)
Apocrine	1 (2)
Receptor status	
TNBC	20 (49)
HER2+ve, ER/PR-ve	7 (17)
HER2+ve, ER/PR+ve	8 (20)
HER2-ve, ER/PR+ve	6 (15)
Associated DCIS	
None	28 (68)
Low grade	0 (0)
Intermediate grade	3 (7)
High grade	10 (24)

Note.—Unless otherwise noted, data are numbers of participants with percentages in parentheses. DCIS = ductal carcinoma in situ, ER = estrogen receptor, HER = human epidermal growth factor receptor, max = maximum, min = minimum, NST = invasive breast cancer, PR = progesterone receptor, TNBC = triple-negative breast cancer.

Table 2: Histopathologic Results and Findings Using MRI, MRE, and the Combined MRI and MRE Methods

End of Treatment Characteristic	Value
Residual cancer burden category	
RCB-0/pCR	23 (56)
RCB-I,II,III	18 (44)
RCB-I	5 (12)
RCB-II	9 (22)
RCB-III	4 (10)
Final MRI	
Complete radiologic response	11 (27)
Partial response	30 (73)
Final MRE prediction	
Complete radiologic response	25 (61)
Partial response	16 (39)
Final MRE and MRI combined prediction	
Complete radiologic response	23 (56)
Partial response	18 (44)

Note.—Data are numbers of participants with percentages in parentheses. MRE = MR elastography, pCR = pathologic complete response, RCB = residual cancer burden.

the receiver operating characteristic curve for DCE MRI, MRE, and a combined approach of DCE MRI and MRE. The receiver operating characteristic analysis resulted in area under the curve, specificity, and sensitivity. In the combined approach a cutoff value was used which was based on the repeatability coefficient. Significance was set at a $P < .05$. All statistical analyses were conducted using SPSS (version 29.0.2.0 [20]; IBM SPSS statistics).

Results

Participant Characteristics

All MRE scans were assessed for quality, as previously described. Participants who did not undergo the complete imaging protocol or failed to meet all criteria were excluded from the analysis. Ultimately, we identified 41 participants who met all criteria for inclusion into the study (Fig 1A) (mean age, 47 years ± 12.5 [SD]; all participants were female). Overall cohort demographics and details regarding tumor types and corresponding receptor status for each included participant are shown in Tables 1, 2, and S1. Histopathologic analysis was used to classify each participant into partial responders or complete responders.

Twenty-three of the 41 participants (56%) achieved pCR. The pathologic response depended on tumor type (X^2 test; $P = .004$), with pCR more likely in triple-negative breast cancer and human epidermal growth factor receptor 2–positive and hormone-negative breast cancers. The pathologic response was also dependent on tumor grade (X^2 test; $P = .02$), with grade 3 tumors more likely to have pCR than grade 2 tumors (Table S2).

Biomechanics and Association with Response or Resistance

The absolute values of elasticity and phase angle for all participants as a function of the NAC regimen are consolidated within Table 3 and Figure S3, with the respective results of the post hoc analysis shown in Table S3. Figure 3 shows maps of elasticity and phase angle at the pre-NAC, post-NAC, and postcycle-1.1 acquisitions for four selected participants who demonstrated response or resistance. These results are quantified in Figure 4 for the entire cohort, which presents TSR and PAR ratios for the relevant time points.

Regarding TSR, response was significantly associated with a drop in relative tumor stiffness at time point 1.1 (Fig 4A) and post-NAC (Fig 4B) acquisitions. Quantitatively, the ratio of elasticity between pre- and post-NAC acquisitions showed a prominent decrease for complete responders (TSR, 0.76 ± 0.16) and an increase for partial responders (TSR, 1.14 ± 0.24). A comparison of both ratios showed a significant difference ($P < .001$) (Fig 5A). As mentioned above, the TSR at time point 1.1 also showed a significant difference between complete and partial responders (complete: TSR, 0.95 ± 0.35 vs partial: TSR, 1.25 ± 0.30; $P = .007$). Figure 5 additionally shows the results as a function of receptor status with, as expected, most pCR belonging to the triple-negative breast cancer and human epidermal growth factor receptor 2–positive and hormone-negative breast cancer groups.

A clear drop in relative phase angle within the tumor region was observed for partial responders compared with complete

Table 3: Average Elasticity and Phase Angle Measurements at Pre-NAC, Postcycle 1.1, and Post-NAC for Participants with Complete and Partial Pathologic Response

Biomechanic and Pathologic Response	Pre-NAC	Postcycle 1.1	Post-NAC
Elasticity (kPa)			
Complete	0.64 ± 0.16	0.61 ± 0.21	0.50 ± 0.18
Partial	0.62 ± 0.14	0.75 ± 0.21	0.70 ± 0.22
Phase angle (0,1)			
Complete	0.28 ± 0.06	0.33 ± 0.07	0.29 ± 0.05
Partial	0.28 ± 0.09	0.26 ± 0.13	0.30 ± 0.05

Note.—Data are means ± SDs. NAC = neoadjuvant chemotherapy.

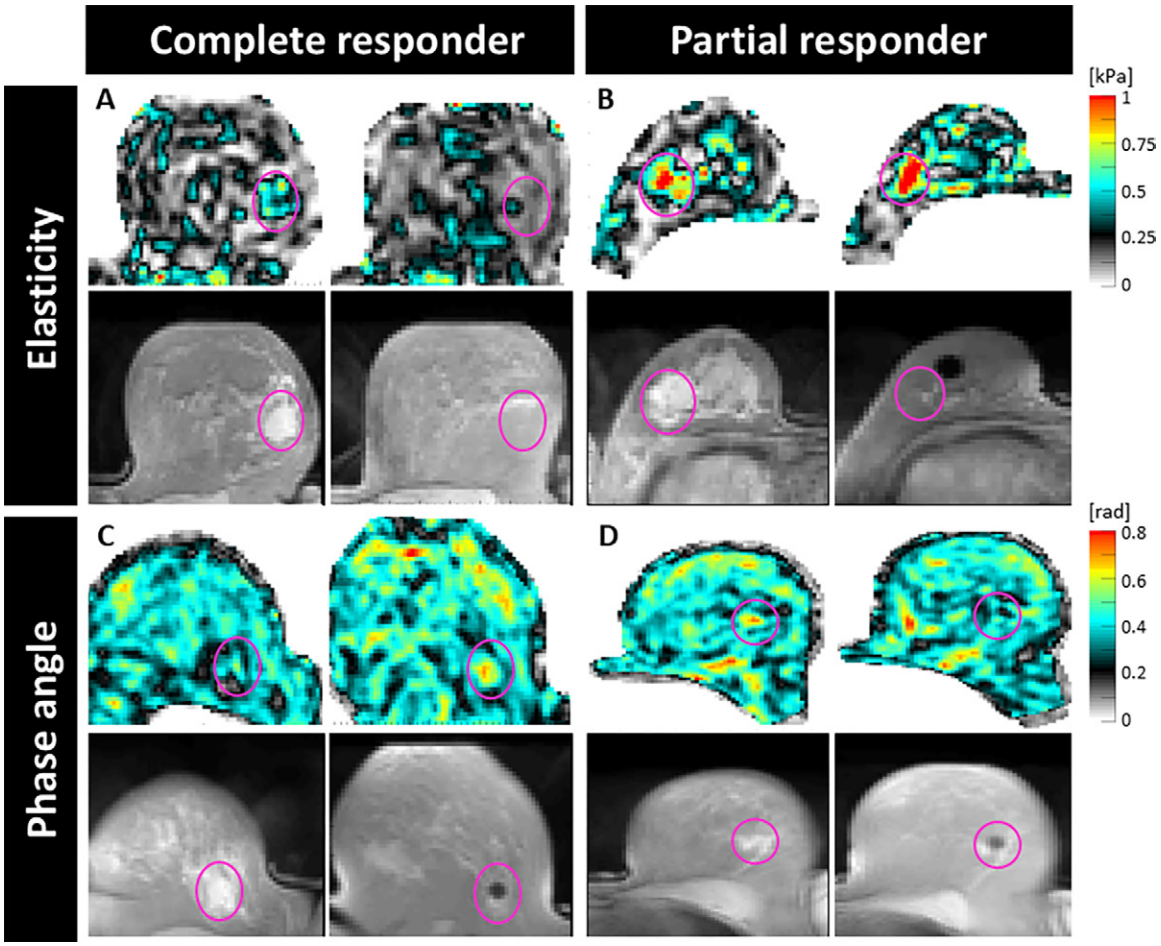

Figure 3: Axial elastograms with corresponding T2-weighted images as examples for biomechanical changes in the tumor region. **(A, B)** Stiffness evolution for a responder (aged 72 years) and partial responder (aged 28 years) from before NAC (left) to after NAC (right), respectively. Response appears to lead to a relative drop in tumor bed stiffness, while resistance leads to a corresponding increase. **(C, D)** Phase angle evolution for a responder (aged 47 years) and partial responder (aged 32 years) from before NAC (left) to time point 1.1 (right), respectively. Response appears to lead to a relative increase in phase angle within the tumor bed, while resistance leads to a corresponding drop.

responders at time point 1.1 (1.23 ± 0.31 vs 0.91 ± 0.34; $P <$ .001), with no evidence of a difference between groups following NAC (1.10 ± 0.29 vs 1.27 ± 0.70; P = .47) (Figs 4, 5).

Figure S3 shows the elasticity and phase angle throughout NAC. Figure S4 shows the elasticity and phase angle prior to NAC as a function of Breast Imaging Reporting and Data System density scores. Furthermore, Figure S5 shows the correlation between PAR and TSR for complete pathologic responders and partial responders.

Repeatability

One participant's repeatability data had to be excluded due to a mechanical failure of the MRE system, leaving 12 participants for the repeatability analysis. The stiffness and phase angle measurements of these participants showed excellent repeatability limits of agreement for elasticity (limits of agreement: -14%, 12%) and for the phase angle (limits of agreement: -12%, 19%) in the tumor. A graphical representation can be found in Figure S6 for the tumorous tissue and apparent healthy tissue taken from the con-

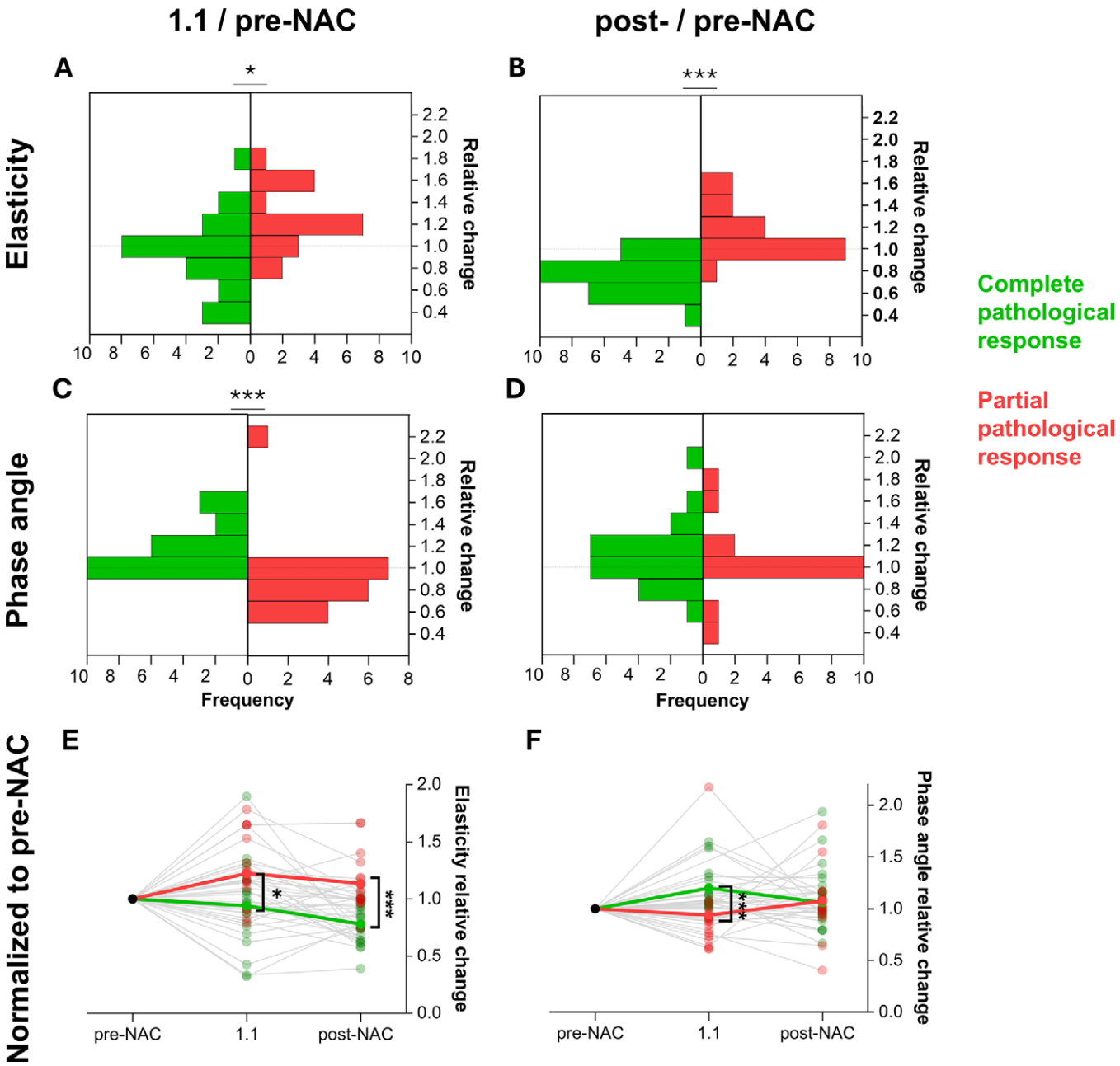

Figure 4: Changes in biomechanics at different time points. **(A–D)** Histograms of the relative change for elasticity for cycle 1.1 and following neoadjuvant chemotherapy (NAC) normalized to before NAC **(A, B)** and phase angle for cycle 1.1 and following NAC normalized to before NAC **(C, D)**, respectively. **(E, F)** Stem plots are shown for the elasticity **(E)** and phase angle **(F)** normalized to before NAC for postcycle 1.1 and following NAC. Note that these measures originate before NAC and after NAC from the tumor footprint while at 1.1 from the tumor region of interest. Green indicates all participants with complete pathologic response and red indicates all participants with partial pathologic response. * $P < .05$, *** $P < .001$.

tralateral side and healthy volunteers who underwent a repeatability protocol with repositioning. Repeatability analysis showed an intraclass correlation coefficient of 0.99 (95% CI: 0.95, 0.99) and a repeatability coefficient of 8.3% for elasticity and an intraclass correlation coefficient of 0.88 (95% CI: 0.59, 0.96) and repeatability coefficient of 5% for the phase angle.

Combined Approach

We compared the current state-of-the-art approach using DCE MRI following NAC for predicting pCR with TSR when using a cutoff value of 1. The corresponding receiver operating characteristic curves are presented in Figure 6A. TSR outperformed the DCE MRI–based approach in terms of area but is less sensitive. DCE MRI had a sensitivity of 94% (95% CI: 74, 100) and a specificity of 44% (95% CI: 26, 63) alone, while TSR yielded a sensitivity of 72% (95% CI: 49, 88) and a specificity of 91% (95% CI: 73, 98). To foster the complementary information provided by both methods, a combined approach was investigated. This relies on determining whether the TSR value surpasses the repeatability coefficient threshold (ie, 8.3%), indicating discernible variances (Fig 6B). In cases where TSR was beyond the interval excluded by the repeatability coefficient (ie, TSR < 0.92 or TSR > 1.08), it was used to predict pCR. Otherwise, when TSR fell into the interval of statistical insignificance (TSR [0.91,1.09]), the classic DCE MRI–based prediction for pCR was used. This dual-biomarker approach provided an elevated specificity of 96%

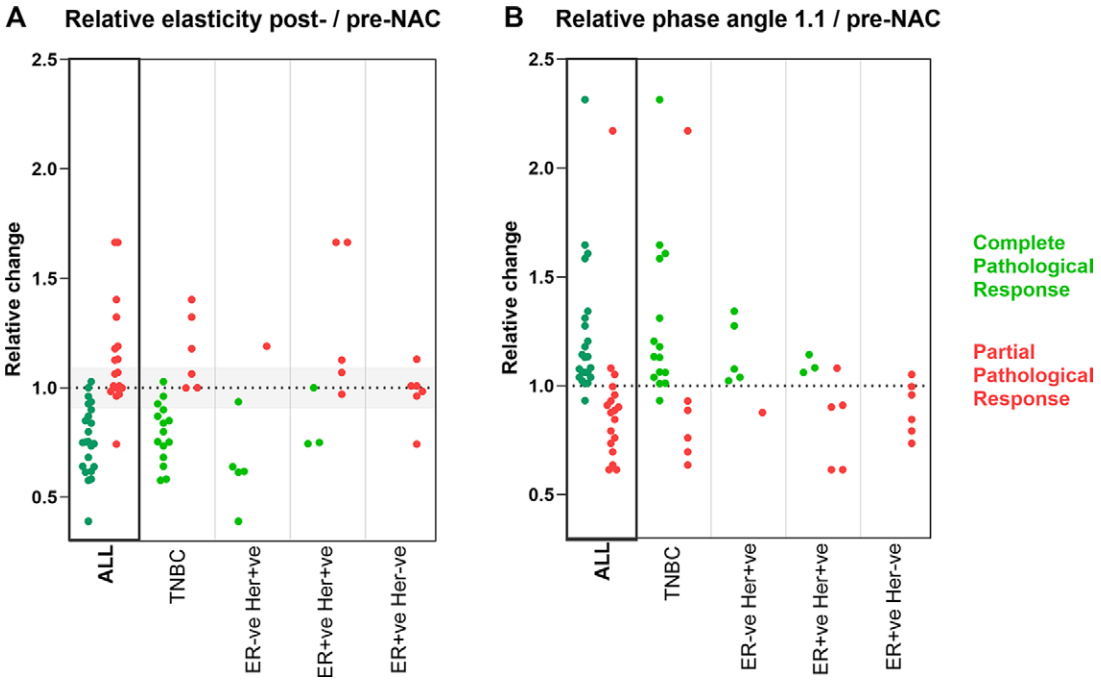

Figure 5: Tumor stiffness and phase angle gauge pathologic response at end–neoadjuvant chemotherapy (NAC) and early at 1.1, respectively. **(A)** The change in tumor bed stiffness at post-NAC relative to pre-NAC is shown for all participants (left) and consecutively as a function of the individual receptor status of the patient. Green circles indicate participants with pathologic complete response, while red circles indicate participants with partial pathologic response (as established from histopathologic analysis after surgery). A stable or rising ratio is indicative of resistance, while a drop in this ratio is indicative of response. As expected, most responders belong to the triple-negative breast cancer (TNBC) receptor status group. The horizontal gray region indicates the repeatability coefficient. **(B)** The change in phase angle within the tumor region after the first cycle (1.1) relative to pre-NAC is shown for all participants (left) and consecutively as a function of the individual receptor status of the patient. Here, a drop in phase angle is indicative of resistance while a rise is indicative of response.

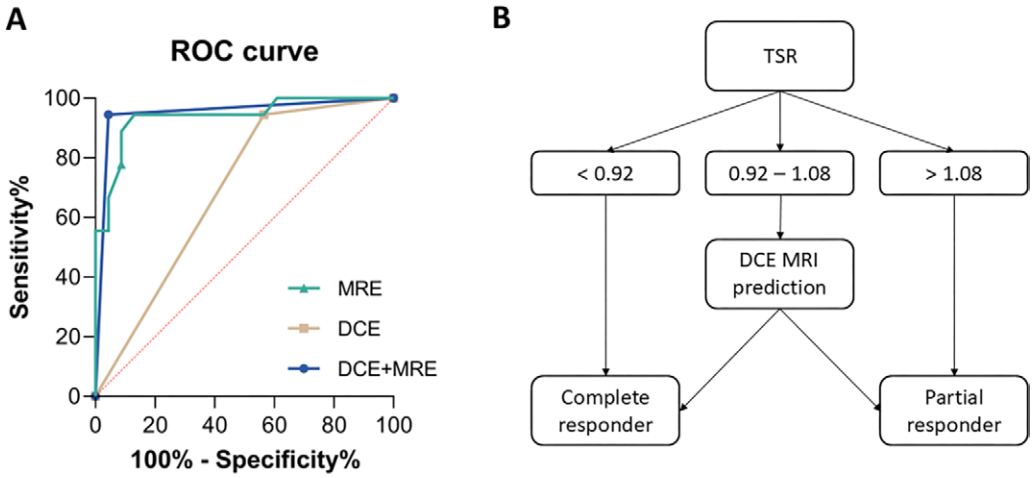

Figure 6: Receiver operating characteristic (ROC) analysis for different predictors of pathologic response. **(A)** ROC curve for different approaches to predict complete pathologic response: tumor stiffness ratio (TSR; green), classic MRI using dynamic contrast-enhanced (DCE) MRI (beige), and dual-approach DCE MRI and MR elastography (MRE; blue). **(B)** Proposed decision pathway to combine DCE MRI at post-NAC and TSR for predicting pathologic response.

(95% CI: 79, 100) while maintaining a high sensitivity of 94% (95% CI: 74, 100) (Fig 6A). The respective area under the receiver operating characteristic curve values were 0.69 (0.53–0.85) (DCE MRI), 0.85 (0.86–1.0) (TSR), and 0.95 (0.87–1.0) (DCE MRI plus MRE). Results are compiled in Table 4.

Discussion

This prospective study evaluated the use of biomechanics (elasticity and phase angle), quantified noninvasively via MRE, to assess response in individuals with breast cancer undergoing NAC. Elasticity alongside standard clinical DCE MRI scans resulted in an increased specificity (44% to 96%) for the prediction of pCR, as assessed by histopathologic analysis, which could potentially be of importance for the de-escalation of surgical intervention. Furthermore, the phase angle showed the possibility of early prediction of pCR (1.23 ± 0.31 vs 0.91 ± 0.34; $P < .001$). Analysis of these two parameters throughout the time course of NAC provided several insights into ther-

Table 4: Diagnostic Performance for Different Predictors of Pathologic Complete Response

Parameter	Final MRI (Post-NAC)	Final MRE (Post-NAC)	Combined MRI and MRE (Post-NAC)	Phase Angle at NAC Cycle 1.1
Sensitivity	94 (74, 100)	72 (49, 88)	94 (74, 100)	83 (61, 94)
Specificity	44 (26, 63)	91 (73, 99)	96 (79, 100)	96 (79, 100)
PPV	57	88	94	93
NPV	91	84	96	85

Note.—Data are percentages with 95% CIs in parentheses. MRE = MR elastography, NAC = neoadjuvant chemotherapy, NPV = negative predictive value, PPV = positive predictive value.

apy-induced changes in biomechanics within the tumor and tumor microenvironment.

First, we found that the replacement of tumorous tissue within the initial tumor footprint by healthy tissue led to drastic changes in mean stiffness upon completion of NAC. Analysis showed that participants with pCR were more likely to exhibit a decrease in stiffness within the tumor footprint following NAC compared with those with partial response. This finding suggests that normal healthy tissue regenerated within the area of the tumor footprint tends to be softer than the initial cancerous tissue. Notably, use of TSR demonstrated a significant association with pCR, and thus, appears to be strongly indicative for pCR.

Second, the relative change in phase angle after the first cycle seems to be highly predictive for pCR, with a drop in relative phase angle indicative of resistance. It is widely noted that resistance leads to fibroblast-induced collagen deposition (29). This theoretically should lead to a drop in phase angle due to the addition of mainly purely elastic composites, which is in accordance with our observation. Fibroblast-induced collagen deposition should concomitantly lead to an increase in stiffness, which is equally observed in our data. Shortly after the first cycle of NAC, there is a disruption of the tumor and its microenvironment resulting in reduction in tumor cell proliferation, increased vascular permeability, edema, tumor necrosis, and inflammation. This results in an increase in osmotic pressure leading to an increase in interstitial fluid pressure, thereby increasing viscosity. This would result in a change in the phase angle at time point 1.1, predicting for complete or partial responders following NAC. This early change is also observed in measurement of elasticity (tumor stiffness) at 1.1 relative to before NAC. While this difference is less prominent than at the end of NAC, it does indicate early tissue alterations regarding biomechanics that correlate to response or resistance, and the rise in elasticity seen for partial responders matches the observed clear drop in phase angle. In addition, recent evidence (30) using transcriptome profiling coupled with histopathologic analyses showed that the first cycle of NAC induced an immune stimulatory response in the microenvironment with upregulation of inflammatory signatures in tumors that was independently associated with a pCR. Furthermore, the first cycle of NAC induced downregulation of cell-cycle genes exemplified by pathways related to cell growth and proliferation.

Third, biomechanics showed higher specificity over the current reference standard clinical MRI using DCE MRI for gauging pCR, with a slightly lower sensitivity. However, a combined biomarker approach of MRE and DCE MRI improved specificity, increasing from 43.5% (DCE MRI alone) to 95.7% (MRE and DCE MRI) while maintaining the high sensitivity of DCE. With the intensively discussed topic of de-escalation of surgery in trials, such as in the phase II trial conducted by Kuerer et al (12), MRE may have an additional role alongside MRI as a noninvasive method to accurately identify patients who have complete clinical response.

There are limitations to our study that should be considered. While the ability to use phase angle as a potential predictor for response or resistance after one cycle of chemotherapy is intriguing, the precise biophysical and biochemical mechanisms underlying the disparity in PAR between complete and partial response remain currently conjectural. Furthermore, response and resistance are gauged via histopathologic analysis after NAC, and this information may not necessarily be representative of changes in biomechanics occurring after one cycle of therapy. Currently, the clinical protocol does not include DCE MRI or additional core biopsies for the quantifications performed at time point 1.1. While findings appear promising, this early patient cohort precludes definitive conclusions. Last, exploring MRE within clinical routine necessitates the incorporation of a mechanical transducer into the radiofrequency coil. Our gravitational transducer setup was well tolerated by all participants with no adverse effects. Additionally, the presence of the transducer paddles fixating the breasts led to reduced motion artifacts than in standard clinical routine data.

To summarize, we have integrated gravitational transducer–based MRE into the clinical workflow of NAC follow-up for individuals with breast cancer and presented three main results: *(a)* a drop in relative tumor bed stiffness observed following NAC was indicative of pCR, *(b)* the combination of this biomechanics-based imaging biomarker with established DCE significantly increased specificity while maintaining the high sensitivity of DCE MRI alone for the identification of complete responders following NAC, and *(c)* a relative change in biomechanical phase angle as early as after the first cycle of NAC was significantly associated with pCR. All three findings warrant further in-depth investigation, including larger (multicenter) cohorts in conjunction with reference standard data through sequential tumor biopsies during NAC. Overall, this study demonstrates the pertinence of biomechanics quantified through noninvasive MRE to provide additional complementary information to clinical decision-making in the context of NAC.

Author affiliations:

[1] School of Cancer and Pharmaceutical Sciences, King's College London, London, United Kingdom

[2] Breast Unit, Guy's and St Thomas NHS Foundation Trust, Guy's Hospital, Great Maze Pond, London SE1 9RT, United Kingdom

[3] School of Biomedical Engineering and Imaging Sciences, King's College London, London, United Kingdom

[4] LVTS, Inserm U1148, University Paris Diderot, Paris, France

[5] Department of Radiology, Guy's and St Thomas NHS Foundation Trust, London, United Kingdom

[6] Breast Unit, King's College Hospital NHS Foundation Trust, London, United Kingdom

Received May 19, 2024; revision requested July 22; revision received November 13; accepted December 13.

Address correspondence to: A.P. (email: arnie.purushotham@kcl.ac.uk).

Funding: Supported by the European Union's Horizon 2020 Societal Challenges Health, Demographic Change, Wellbeing Programme (grant agreement no. 668039), and the Cancer Research UK and Department of Health as Experimental Cancer Medicine Centres. Cancer Research UK Award ECMCQQR-2022/10005 new award for ECMC from March 2023 to March 2028.

Author contributions: Guarantors of integrity of entire study, **A.P.S., B.S., Z.P., K.W., H.H., E.S., A.S., R.S., A.P.**; study concepts/study design or data acquisition or data analysis/interpretation, all authors; manuscript drafting or manuscript revision for important intellectual content, all authors; approval of final version of submitted manuscript, all authors; agrees to ensure any questions related to the work are appropriately resolved, all authors; literature research, **A.P.S., P.J., O.D., K.W., V.K., A.S., T.N., R.S., A.P.**; clinical studies, **A.P.S., P.J., A.S.v.S., O.D., B.S., G.A., Z.P., H.J., K.W., A.M., J.S., A.K., H.H., G.B., V.K., E.S., A.S., A.R., S.P., R.S., A.P.**; statistical analysis, **A.P.S., P.J., A.S.v.S., H.J., R.S.**; and manuscript editing, **A.P.S., P.J., A.S.v.S., O.D., K.W., A.K., H.H., E.S., A.S., A.R., R.S., A.P.**

Data sharing: Data generated or analyzed during the study are available from the corresponding author by request.

Disclosures of conflicts of interest: A.P.S. No relevant relationships. **P.J.** No relevant relationships. **A.S.v.S.** No relevant relationships. **O.D.** No relevant relationships. **B.S.** No relevant relationships. **G.A.** No relevant relationships. **Z.P.** No relevant relationships. **H.J.** No relevant relationships. **K.W.** No relevant relationships. **A.M.** No relevant relationships. **J.S.** No relevant relationships. **A.K.** No relevant relationships. **H.H.** No relevant relationships. **G.B.** No relevant relationships. **V.K.** No relevant relationships. **M.T.** Data safety monitoring board member of multiple clinical trials (ADD-Aspirin, CaPP3, GISTAR, COLO-PREVENT, TARGIT-B, TOGAS); steering committee member of multiple societies (International Cancer Prevention Society, UK Therapeutic Cancer Prevention Network, Cancer Prevention Europe, European Code Against Cancer 5 working group, Advisory Committee on Clinical Impact Awards sub-committee, The Norwegian Cancer Society, Research Peer-Review Committee Cancer Research UK, Prevention and Population Research Committee Expert Review Panel [ad hoc member]). **E.S.** No relevant relationships. **A.S.** No relevant relationships. **A.R.** No relevant relationships. **T.N.** Grants from EU IMI2, CRUK City of London Cancer Centre: a UCL-Barts-King's-Crick CRUK Major Centre initiative, GSK-KCL Translational Oncology Research Hub, CRUK Early Detection and Diagnosis (ED&D) Programme, UCB, Incyte Corporation, Cancer Research UK Early Detection Committee, Cancer Research UK Wellcome Trust, Wellcome Leap, and National Cancer Imaging Translational Accelerator; part-time employee of GSK but this manuscript entirely relates to KCL appointment and the findings bear no impact or relationship to work within GSK. **S.P.** Grants from the National Institute for Health Research, Guy's & St Thomas' Charity, Medical Research Council, Wellcome Leap, Butterfield Trust, and Cancer Research UK; payment for educational events from Exact Science, Daiichi-Sankyo, Roche, and AstraZeneca; travel support from Exact Science, India Breast Meeting 2024, Roche, and AstraZeneca; advisory board member for Exact Science; independent data monitoring committees for POETIC-A and c-TRAK TN in the last 3 years; chair of the UK National Coordinating Committee for Breast Pathology and president of the Association of Breast Pathology (both unpaid). **R.S.** No relevant relationships. **A.P.** Grants from Wellcome LEAP, Cancer Research UK, Medical Research Council, and Guy's Cancer Charity; leadership roles with Maggie's Charity and Richard Dimbleby Cancer Fund Charity.

References

1. Arnold M, Morgan E, Rumgay H, et al. Current and future burden of breast cancer: Global statistics for 2020 and 2040. Breast 2022;66:15–23.
2. Lifetime risk estimates calculated by the Cancer Intelligence Team at Cancer Research UK. https://www.cancerresearchuk.org/health-professional/cancer-statistics/statistics-by-cancer-type/breast-cancer/risk-factors#heading-Zero. Published 2023. Updated December 14, 2023. Accessed 2024.
3. Simon A, Robb K. Cancer: breast. In: Ayers S, Baum A, McManus C, et al, eds. Cambridge Handbook of Psychology, Health and Medicine. 2nd ed. Cambridge University Press, 2022; 577–580.
4. Yau C, Osdoit M, van der Noordaa M, et al. Residual cancer burden after neoadjuvant chemotherapy and long-term survival outcomes in breast cancer: a multicentre pooled analysis of 5161 patients. Lancet Oncol 2022;23(1):149–160.
5. Cheng Q, Huang J, Liang J, et al. The Diagnostic Performance of DCE-MRI in Evaluating the Pathological Response to Neoadjuvant Chemotherapy in Breast Cancer: A Meta-Analysis. Front Oncol 2020;10:93.
6. Lord SJ, Lei W, Craft P, et al. A systematic review of the effectiveness of magnetic resonance imaging (MRI) as an addition to mammography and ultrasound in screening young women at high risk of breast cancer. Eur J Cancer 2007;43(13):1905–1917.
7. Menezes GLG, Knuttel FM, Stehouwer BL, Pijnappel RM, van den Bosch MAAJ. Magnetic resonance imaging in breast cancer: A literature review and future perspectives. World J Clin Oncol 2014;5(2):61–70.
8. Shahid H, Wiedenhoefer JF, Dornbluth C, Otto P, Kist K. An overview of breast MRI. Appl Radiol 2016;45(10):7–13. https://scholars.uthscsa.edu/en/publications/an-overview-of-breast-mri.
9. Hariharan N, Rao TS, Rajappa S, et al. Accuracy of Tumor Bed Biopsy for Predicting Pathologic Complete Response After Chemotherapy Among Women With Breast Cancer: Complete Responders in the Breast Study. JCO Glob Oncol 2023;9(9):e2300014.
10. Rauch GM, Kuerer HM, Adrada B, et al. Biopsy Feasibility Trial for Breast Cancer Pathologic Complete Response Detection after Neoadjuvant Chemotherapy: Imaging Assessment and Correlation Endpoints. Ann Surg Oncol 2018;25(7):1953–1960.
11. Teoh V, MacNeill F, Roche N, et al. Image-guided vacuum-assisted biopsy to assess pathologic complete response in breast cancer patients with exceptional response to neoadjuvant chemotherapy. J Glob Oncol 2019;5(suppl):39.
12. Kuerer HM, Smith BD, Krishnamurthy S, et al. Eliminating breast surgery for invasive breast cancer in exceptional responders to neoadjuvant systemic therapy: a multicentre, single-arm, phase 2 trial. Lancet Oncol 2022;23(12):1517–1524.
13. Chang JM, Moon WK, Cho N, et al. Clinical application of shear wave elastography (SWE) in the diagnosis of benign and malignant breast diseases. Breast Cancer Res Treat 2011;129(1):89–97.
14. Dvorak HF, Weaver VM, Tlsty TD, Bergers G. Tumor microenvironment and progression. J Surg Oncol 2011;103(6):468–474.
15. Avraamides CJ, Garmy-Susini B, Varner JA. Integrins in angiogenesis and lymphangiogenesis. Nat Rev Cancer 2008;8(8):604–617.
16. Levental KR, Yu H, Kass L, et al. Matrix crosslinking forces tumor progression by enhancing integrin signaling. Cell 2009;139(5):891–906.
17. Nguyen DX, Bos PD, Massagué J. Metastasis: from dissemination to organ-specific colonization. Nat Rev Cancer 2009;9(4):274–284.
18. Swartz MA, Kaipainen A, Netti PA, et al. Mechanics of interstitial-lymphatic fluid transport: theoretical foundation and experimental validation. J Biomech 1999;32(12):1297–1307.
19. Acerbi I, Cassereau L, Dean I, et al. Human breast cancer invasion and aggression correlates with ECM stiffening and immune cell infiltration. Integr Biol 2015;7(10):1120–1134.
20. Samani A, Bishop J, Luginbuhl C, Plewes DB. Measuring the elastic modulus of ex vivo small tissue samples. Phys Med Biol 2003;48(14):2183–2198.
21. Samani A, Zubovits J, Plewes D. Elastic moduli of normal and pathological human breast tissues: an inversion-technique-based investigation of 169 samples. Phys Med Biol 2007;52(6):1565–1576.
22. Muthupillai R, Lomas DJ, Rossman PJ, Greenleaf JF, Manduca A, Ehman RL. Magnetic resonance elastography by direct visualization of propagating acoustic strain waves. Science 1995;269(5232):1854–1857.
23. Sinkus R, Siegmann K, Xydeas T, Tanter M, Claussen C, Fink M. MR elastography of breast lesions: understanding the solid/liquid duality can improve the specificity of contrast-enhanced MR mammography. Magn Reson Med 2007;58(6):1135–1144.
24. Balleyguier C, Lakhdar AB, Dunant A, Mathieu MC, Delaloge S, Sinkus R. Value of whole breast magnetic resonance elastography added to MRI for lesion characterization. NMR Biomed 2018;31(1):e3795.
25. Patel BK, Samreen N, Zhou Y, et al. MR Elastography of the Breast: Evolution of Technique, Case Examples, and Future Directions. Clin Breast Cancer 2021;21(1):e102–e111.
26. Runge JH, Hoelzl SH, Sudakova J, et al. A novel magnetic resonance elastography transducer concept based on a rotational eccentric mass: preliminary experiences with the gravitational transducer. Phys Med Biol 2019;64(4):045007.
27. Garteiser P, Sahebjavaher R, Sinkus R, et al. Rapid 3D periodic motion-encoding using steady-state FFE pulse sequence: application towards multi-frequency rheology. In: 20th Annual Meeting of the International Society for Magnetic Resonance in Medicine. International Society for Magnetic Resonance in Medicine, 2012; 3423. https://archive.ismrm.org/2012/3423.html.
28. Sinkus R, Lambert S, Abd-Elmoniem KZ, et al. Rheological determinants for simultaneous staging of hepatic fibrosis and inflammation in patients with chronic liver disease. NMR Biomed 2018;31(10):e3956.
29. Xu S, Xu H, Wang W, et al. The role of collagen in cancer: from bench to bedside. J Transl Med 2019;17(1):309.
30. Park YH, Lal S, Lee JE, et al. Chemotherapy induces dynamic immune responses in breast cancers that impact treatment outcome. Nat Commun 2020;11(1):6175.